Arunachalam et al., *Cogent Physics* (2015), 2: 1067344
http://dx.doi.org/10.1080/23311940.2015.1067344

cogent physics

MATERIALS SCIENCE | RESEARCH ARTICLE

Ultrasonic studies on sodium-doped $LaMnO_3$ perovskite material

M. Arunachalam[1], P. Thamilmaran[1], S. Sankarrajan[2] and K. Sakthipandi[3]*

Received: 05 March 2015
Accepted: 22 June 2015
Published: 17 July 2015

*Corresponding author: K. Sakthipandi, Department of Physics, Sethu Institute of Technology, Kariapatti 626 115, Tamil Nadu, India
E-mail: sakthipandi@gmail.com

Reviewing editor:
Rajeev Ahuja, Uppsala University, Sweden

Additional information is available at the end of the article

Abstract: $La_{1-x}Na_xMnO_3$ perovskite manganite in the form of circular pellets was prepared with the composition of x = 0.10, 0.15 and 0.20 by the solid-state reaction technique. To confirm the crystalline nature of the samples, X-ray diffraction patterns of the samples were obtained. It is found that the samples have a rhombohedral structure with R3c space group. Particle size was determined from the obtained scanning electron microscope images. Ultrasonic velocity and the attenuation measurements were carried out on the samples employing the transmission technique in the temperature range from 300 to 400 K. The anomalous behaviour obtained in the ultrasonic measurements was used to explore the transition temperature of the prepared $La_{1-x}Na_xMnO_3$ perovskite samples. The temperatures 320, 328 and 334 K are the ferromagnetic to paramagnetic phase transition temperatures of the samples x = 0.10, 0.15 and 0.20, respectively.

Subjects: Electromagnetics & Communication; Engineering & Technology; Ultrasonics

Keywords: perovskite manganite materials; ultrasonic measurement; phase transition

ABOUT THE AUTHORS

The authors M. Arunachalam and P. Thamilmaran are associate professors of Physics in Sri S.R.N.M. College, Sattur, Tamil Nadu, India. S. Sankarrajan is working as a professor of Physics in Unnamalai Institute of Technology, Kovilpatti, Tamil Nadu, India.

K. Sakthipandi is an assistant professor of Physics, Sethu Institute of Technology, Kariapatti, Tamil Nadu, India. He is the principal investigator of two sponsored projects funded by the Department of Science and Technology, government of India. His main area of interest is the characterisation of structural materials employing *in situ* ultrasonic studies. An indigenously designed experimental set-up is used for the *in situ* measurement of ultrasonic velocity and attenuation over wide range of temperatures. The marked softened and hardened lattices are used to explore the temperature-dependent phase transition. The development and improvement of perovskite manganites are required for potential applications such as solid oxide fuel cells, magnetic sensors/reading heads and frequency switching devices.

PUBLIC INTEREST STATEMENT

Ultrasonics is an area of intense scientific and technological research. Due to its scientific and engineering applications, it has drawn considerable attention of researchers. Perovskites are advanced materials which find wider applications in frequency switching devices, sensor technology, solar cells, magnetic storage devices/heads, etc. due to their physicochemical properties and complex phase diagrams. Even though different techniques such as electrical resistivity, magnetoresistance, magnetization and specific heat measurements are available, in situ ultrasonic measurement is an effective tool to explore the temperature-dependent phase transitions. This is possible due to the interaction of ultrasonic waves with macro/micro/submicroscopic lattice of the materials. In the present investigation, the phase transition of the sodium-doped lanthanum perovskite manganite was explored. Identification of structural/microstructural transitions and the influence of temperature are important parameters for both development of materials and useful guidelines to the design engineers to set acceptable limits for service conditions.

1. Introduction

In recent years, advance materials such as perovskite manganite with the general formula $R_{1-x}A_xMnO_3$ (R—rare earth element and A—doping elements such as Sr, Ba, Ca, Na and K) assume significant importance in view of their special physical properties such as colossal magneto resistance (CMR), metal–insulator (MI) phase transition and ferromagnetic (FM) to paramagnetic (PM) phase transition (Lalitha & Reddy, 2009; Park et al., 1998; Tokura, 1997). These special properties along with higher chemical stability, lower eddy current heating, tunable Curie temperature (T_c) that can be spanned over a wide range of temperature and low cost make them significant in applications such as frequency switching devices, sensor technology, solar cells and so on (Chand, Kumar, & Varma, 2011; Paul & Paul, 2014; Wang, Xu, Sun, Pan, & Zhang, 2011). In $R_{1-x}A_xMnO_3$ perovskite manganite compounds, the oxygen is in the O^{2-} state and Mn has two oxidation states viz. Mn^{3+} and Mn^{4+}. The doping of divalent materials causes a change in the valence of Mn ions from 3 to 4. The charge and spin exchanges between the Mn^{3+} and Mn^{4+} ions via O^{2-} is called the double exchange (DE) interaction, which is primarily the cause of the interesting magnetic and electrical properties exhibited by these materials (Likodimos & Pissas, 2005; Taguchi, 1998; Zener, 1951).

The doping of divalent Sr changes $LaMnO_3$ perovskite manganite from antiferromagnetic (AFM) insulator state to FM metallic state is caused by the increase in the number of holes from Mn^{3+} to Mn^{4+}. The CMR effect around the FM to PM phase transition temperature (T_C) is due to the mixed valence of Mn caused by the Mn^{3+} in $LaMnO_3$ to Mn^{4+} in the doped $SrMnO_3$ (de Gennes, 1960; De Teresa et al., 1995). Hence, the observed magnetic and electronic phase diagrams of the mixed valent perovskite manganite materials could not be explained with the DE interaction theory alone. Besides the DE interaction, there are few other phenomena such as charge and orbital instabilities, electron-lattice, spin-lattice coupling (Millis, 1995; Zheng, Zhu, Xie, Huang, & Zi, 2002), Jahn–Teller (JT) interaction, charge-orbital ordering, AFM super exchange interaction (Chen & Cheong, 1996; Radaelli, Cox, Marezio, & Cheong, 1997) that also play a role in their properties.

Survey of literature on the mixed valent perovskites has shown that in most of the studies, the divalent alkaline elements such as strontium and calcium were used as the dopant (Jaafar & Abd Shukor, 2003; Tang & Zhang, 2006). However, only a small amount of work was carried out on monovalent alkali elements such as sodium lithium, potassium, etc. as the doping materials in the study of perovskites (Kalyana Lakshmi, Venkataiah, Vithal, & Venugopal Reddy, 2008; Roy, Guo, Venkatesh, & Ali, 2001; Zhong et al., 1998). Monovalent alkali elements having only one electron in the outer most orbit are more reactive than the divalent alkaline elements. Further, monovalent alkali elements such as sodium, potassium, etc. have more pronounced donor properties than the divalent alkaline materials. When a monovalent element is doped in a perovskite compound of $R_{1-x}A_xMnO_3$, for every amount of x of A (alkali) element, an amount $2x$ of Mn^{3+} will be converted into Mn^{4+}. Ultimately, the distribution of valency is given by $R^{3+}_{1-x}A^{+}_{x}(Mn^{3+}_{1-2x}Mn^{4+}_{x}O_3$ (Roy et al., 2001). This facilitates the production of a large number of charge carriers and a significant increase in conductivity. Further, the ratio between Mn^{3+} and Mn^{4+} leads to the enhancement of the DE interaction favouring ferromagnetism (Roy et al., 2001). So, one can expect perovskite materials doped with alkali materials to show distinguishing behaviour in the electronic, magnetic and structural properties than the materials doped with the alkaline elements (Zhong et al., 1998).

When the monovalent potassium is doped in $La_{1-x}A_xMnO_{3+\delta}$, the average ionic radius of the La site increases and produces a crystallographic distortion that leads to an increase in Mn–O–Mn bond angle. This in turn causes a shortening of Mn–O distance. Hence, a stronger DE interaction associated with an increase in the Curie temperature T_c is produced (Zhong et al., 1998). In the present study, the aim is to use a monovalent alkali element i.e. sodium as the doping material in $LaMnO_3$ perovskite manganite materials and explore the structural/phase transition properties of the samples.

The four-probe electrical resistivity measurements made on $La_{0.67}A_{0.33}MnO_3$ (A—Alkali element Li and Na) revealed the metal–insulator transition temperature (T_{MI}) is 130 and 220 K for Li and Na, respectively (Kalyana Lakshmi et al., 2008). The X-ray diffraction (XRD) analysis on $La_{1-x}Na_xMnO_3$

perovskite manganite samples prepared by the solid-state reaction method revealed an increase in Mn–O–Mn bond angle and a decrease in Mn–O bond length with the increase in the doping concentration Na (Ye et al., 2001). The value of T_C in the potassium-doped $La_{1-x}K_xMnO_3$ (x = 0.05, 0.10 and 0.15) perovskite manganites strongly depends on the content of potassium and is in between 260 and 309 (Das & Dey, 2007).

The VSM studies made on $La_{0.7}Ca_{0.3-x}Na_xMnO_3$ (x = 0, 0.04 and 0.08) perovskite samples show that the value of T_C increases from 276 to 289 K with the increase in sodium content from 0.04 to 0.08 (Tovstolytkin, Pogorily, & Podyalvski, 2007). Zhu, Sun, Dai and Song (2006) reported that super conducting quantum interference device magnetometer (SQUID) studies made on the $La_{0.8}Na_{0.2}MnO_3$ perovskite manganite materials revealed that the value of T_{MI} (354 K) is much greater than the value of T_C (333 K).

Being a non-destructive technique, ultrasonic measurement attracts considerable importance for the characterisation of the materials. Quite a number of researches were carried out to study the phase transition and related properties of perovskite materials using ultrasonic parameters. A dramatic softening of ultrasonic velocities and a sharp peak in attenuation were observed at 234 K around the phase transition in $Nd_{0.67}Sr_{0.33}MnO_3$ perovskite manganite sample (Arunachalam, Thamilmaran, Sankarrajan, & Sakthipandi, 2015).

Therefore, the aim is to study $La_{1-x}Na_xMnO_3$ (x = 0.10, 0.15 and 0.20) perovskite manganite samples using different characterisation techniques such as X-ray diffractometry, scanning electron microscope (SEM) and energy dispersive analysis of X-rays (EDX). The temperature dependence of ultrasonic velocities and attenuation were measured over a wide range of temperature in order to explore the phase transition in the prepared perovskite manganite samples.

2. Experimental procedure

2.1. Sample preparation

$La_{1-x}Na_xMnO_3$ perovskite manganite materials with the composition of x = 0.10, 0.15 and 0.20 were prepared by employing the solid-state reaction technique. Pure grade manganese carbonate (99.99%; Sigma–Aldrich), lanthanum nitrate (99.99%; Sigma–Aldrich) and sodium nitrate (99.0%; HiMedia GR, India) powders were taken in stoichiometric quantity and weighed on a digital balance. Then, the powders were mixed in an agate mortar. The mixture was calcinated two times at 873 K in air for 2 h and further ground to obtain a homogeneous mixture. Once again, the mixture was calcinated at 873 K in air for 2 h and then the obtained powder was pressed into pellets of diameter 12 mm and thickness, 4 mm with a stainless steel dye. The pellets were sintered at 1,373 K for 12 h in atmospheric air. Thus, the samples were prepared in the form of pellets. Hereafter, the samples will be notified as LNMO10, LNMO15 and LNMO20 for the composition x = 0.10, 0.15 and 0.20 in the $La_{1-x}Na_xMnO_3$ perovskite manganite samples, respectively.

2.2. Density

Density of the samples was determined using Archimedes principle. The pellets were weighed in air (W_a) and in buoyant CCl_4 (W_b) using the formula (Arunachalam et al., 2015; Zhu et al., 2006)

$$\rho = \frac{W_a \rho_b}{W_a - W_b} \tag{1}$$

where ρ_b is the density of the buoyant.

2.3. X-ray diffractometry

The crystalline nature of the prepared LNMO perovskite manganite samples was obtained by the recorded XRD patterns using a powder X-ray diffractometer (X'PERT PRO PANalytical, Netherland) with Cu–K_α as the source of radiation. The scanning range was 10–80° with an increment of 0.05°.

2.4. Microscopic studies

Spectral images obtained from the SEM coupled with the EDX (JEOL, JED 5300) were used to study the surface images and the elemental composition of the prepared LNMO perovskite manganite samples.

2.5. Ultrasonic measurements

An indigenously designed experimental set-up was used to measure the ultrasonic velocity and attenuation over a wide range of temperature starting from 300 to 400 K with the help of a programmable temperature controller (Eurotherm, 2604, USA). A high-power ultrasonic pulse receiver (Olympus NDT, 5900PR, USA) was used for the transmission and reception of the ultrasonic signals. For recording the digital RF ultrasonic signals, a computer-in-built 1-GHz digital storage oscilloscope (Lecroy, Wave Runner 104Mxi, USA) was used. *X* and *Y* cut transducers operating at a fundamental frequency of 5 MHz were used, respectively, to produce longitudinal and shear ultrasonic waves. Similar procedure was adopted to measure longitudinal ultrasonic velocity (U_L) and shear ultrasonic velocity (U_S) as reported in the earlier study (Arunachalam et al., 2015; Sakthipandi & Rajendran, 2013). The temperature required was kept under the dynamic mode of operation. The error in temperature measurement was ±1 K. A standard procedure was used to carry out couplant (Sakthipandi & Rajendran, 2013) and zero porosity (Thamilmaran, Arunachalam, Sankarrajan, & Sakthipandi, 2015) corrections for the measured velocity and attenuation measurement. Elastic constants such as longitudinal (*L*), shear (*G*) bulk (*K*), Young's (*E*) modulus and Poisson's ratio (σ) and the first-order differential function of ultrasonic parameters were obtained using standard relations (Sakthipandi & Rajendran, 2013).

3. Results and discussion

The obtained XRD patterns of the prepared LNMO perovskite manganite samples are shown in Figure 1. The crystalline nature of the samples was confirmed by the sharp peaks seen in the spectra. The values of the diffraction angles are in close agreement with the rhombohedral structure with R3c space group (JCPDS files 89-8122 and 89-8028). The crystal size of the prepared samples was calculated using Scherrer's formula (Arunachalam et al., 2015) using the obtained 2θ and full width half maximum (FWHM) values of the peaks. The crystalline size of the samples is 42.635, 35.973 and 29.848 nm for LNMO10, LNMO15 and LNMO20 perovskite manganite samples, respectively. From this, it is revealed that the crystalline size decreases as the doping level of Na increases.

The elemental composition of the constituents of the prepared LNMO10, LNMO15 and LNMO20 perovskite manganite samples was obtained from the energy EDX patterns shown in Figure 2. The EDX measurement ensures that the atomic ratio of the elements La, Na, Mn and O atoms are matching with that of the nominal composition of the prepared LNMO perovskite manganite samples. The

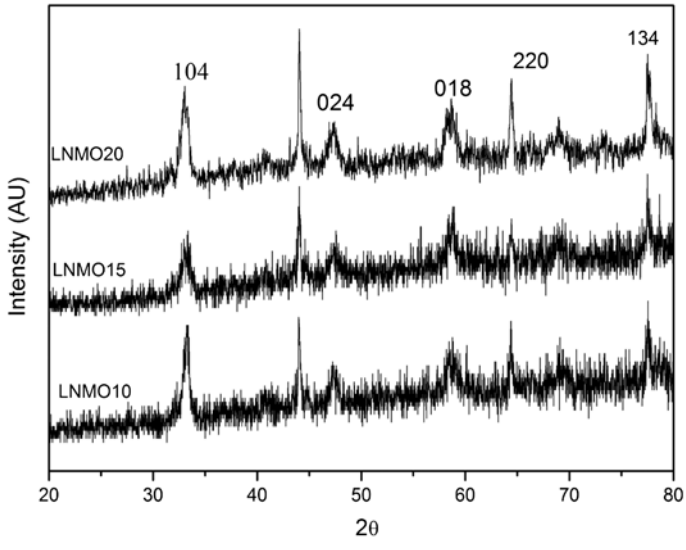

Figure 1. XRD spectrum of the LNMO samples.

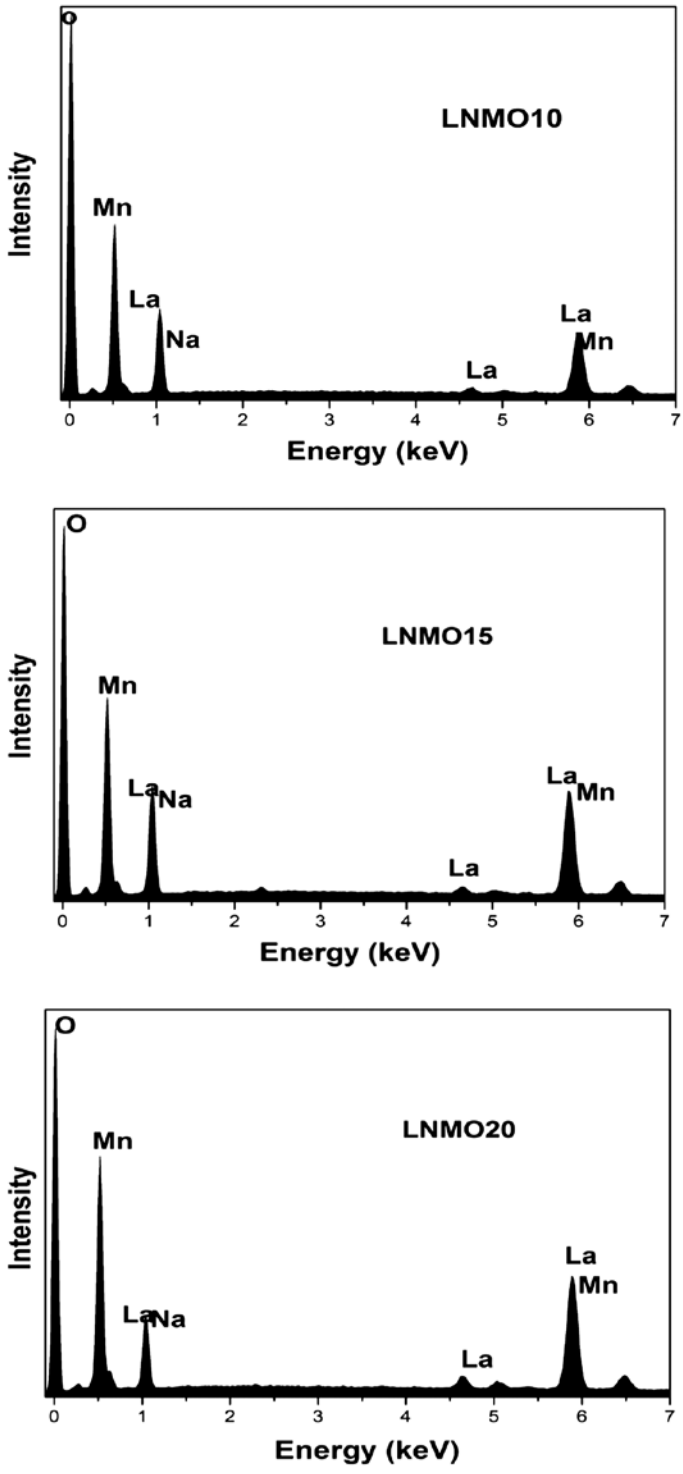

Figure 2. EDX pattern of the LNMO samples.

SEM images of the samples shown in Figure 3 reveal an agglomeration and morphology of the particles. The approximate particle size of the samples is determined using the SEM images taking into account the minimum and maximum diameter of the large number of particles. The particle size of the samples LNMO10, LNMO15 and LNMO20 perovskite manganite samples is 193.3, 155.5 and 143.3 nm, respectively. From this data, it is inferred that the particle size decreases as the doping

Figure 3. SEM pattern of the LNMO samples.

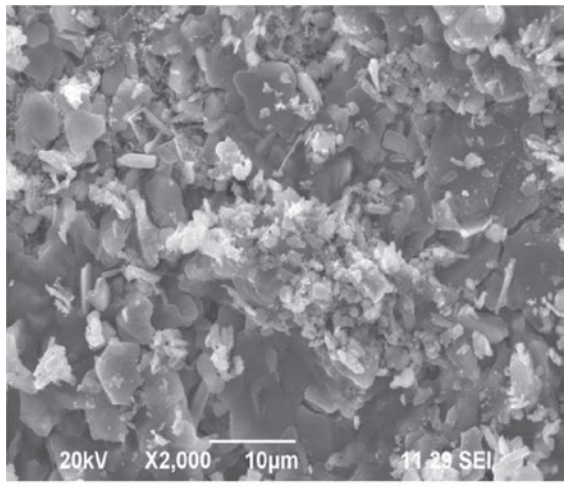

LNMO10

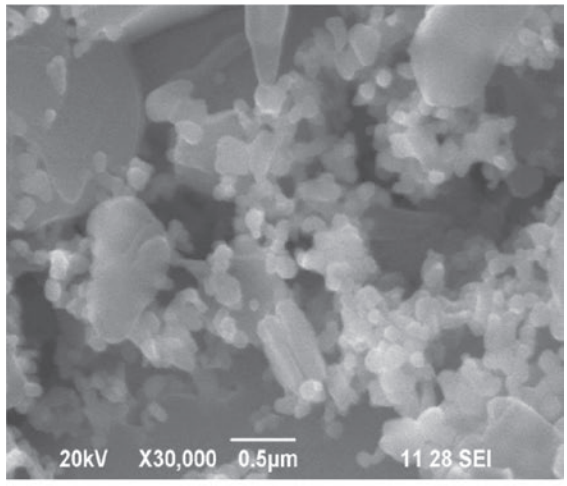

LNMO15

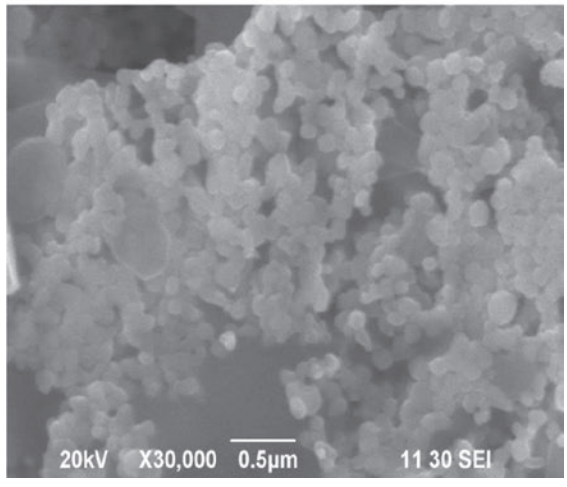

LNMO20

level of Na increases. The density of the samples is 5,213, 5,329 and 5,467 kgm^{-3} for LNMO10, LNMO15 and LNMO20, respectively.

The values of the physical quantities such as crystal size, particle size, density (ρ), and ultrasonic parameters such as longitudinal velocity (U_L), shear velocity (U_S) and their respective attenuation (α_L and α_S) measured at the room temperature 300 K along with that of the elastic constants *L*, *G*, *K* and *E* are given in Table 1. It is observed from Table 1 that when the concentration of the monovalent doping element Na increases, the velocity of ultrasonic waves in both the longitudinal and the shear mode decreases. The longitudinal velocity of the samples at 300 K is 5,935, 5,739 and 5,525 m s^{-1} for the LNMO10, LNMO15 and LNMO20 samples, respectively. As far as the attenuation is concerned, a reverse trend is observed. The respective attenuation values are 1.3395, 1.3922 and 1.4705 dB cm^{-1}. This behaviour is ascribed to the increase in density caused by the decrease in lattice parameters that appeared as the composition of sodium increases in the samples. Further, a decrease in ultrasonic velocity and an increase in attenuation lead to an increase in acoustical activation energy (E_P). The increase in E_P along with the thermally activated structural relaxation is the reason behind the dip/peak in the ultrasonic parameters (Ye et al., 2001). Similar trend to that of velocity was observed in the case of elastic constants (*L*, *G*, *K* and *E*) also.

Temperature-dependent measurement of the ultrasonic parameters is a vital tool that is used to study the structural and phase transitions in the perovskite (Jaafar & Abd Shukor, 2003). When ultrasonic measurements are carried out over a wide range of temperature in perovskite manganite samples, an anomaly is observed in the region where the structural/magnetic phase transition takes place (Sakthipandi & Rajendran, 2013; Tang & Zhang, 2006; Thamilmaran et al., 2015). In this investigation, the ultrasonic parameters such as U_L, U_S, α_L and α_S were measured employing the transmission

Table 1. Physical and ultrasonic parameters of the LNMO samples at 300 K

Parameters	LNMO10	LNMO15	LNMO20
Crystal size (XRD) nm	42.635	35.973	29.848
Particle size (SEM) nm	193.3	155.5	143.3
Density kgm^{-3}	5,213	5,329	5,467
Longitudinal velocity (U_L) m s^{-1}	5,935	5,739	5,525
Shear velocity (U_S) m s^{-1}	2,982	2,921	2,863
Long. attenuation (α_L) $dBcm^{-1}$	1.3395	1.3922	1.4706
Shear attenuation (α_S) $dBcm^{-1}$	7.4977	7.8616	8.1426
Longitudinal modulus (*L*) GPa	183.6239	175.5166	166.8836
Shear modulus (*G*) GPa	46.3557	45.4683	44.8117
Bulk modulus (*K*) GPa	121.8318	114.9073	107.1495
Young's modulus (*E*) GPa	123.4127	120.508	117.9851

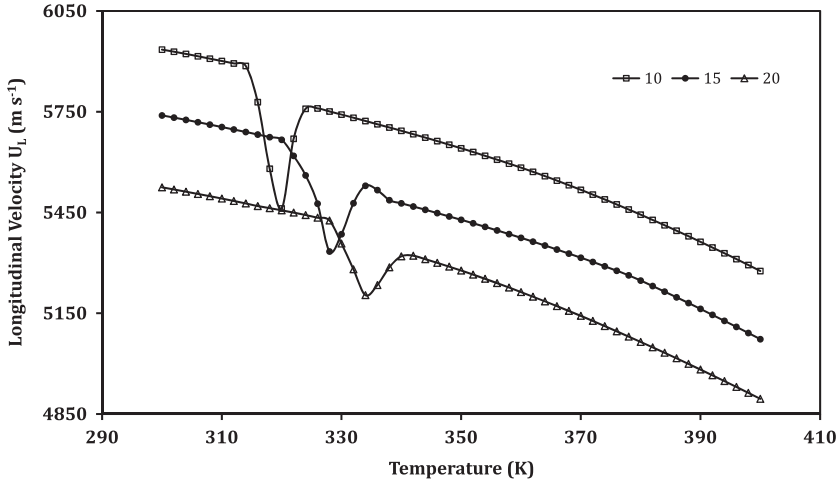

Figure 4. Variation of longitudinal velocity (U_L) with temperature in the LNMO samples.

technique in the temperature range from 300 to 400 K. The temperature dependence of the ultrasonic parameters measured is shown in Figures 4–8. From Figure 4, it is seen that the longitudinal

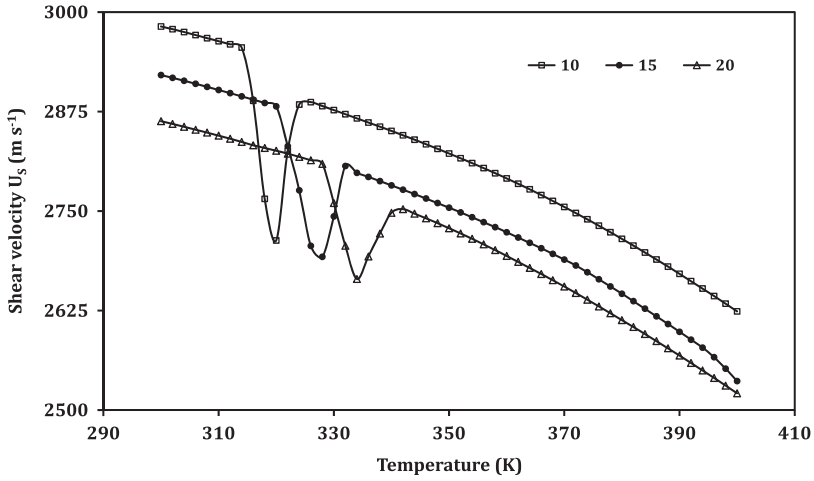

Figure 5. Variation of shear velocity (U_s) with temperature in the LNMO samples.

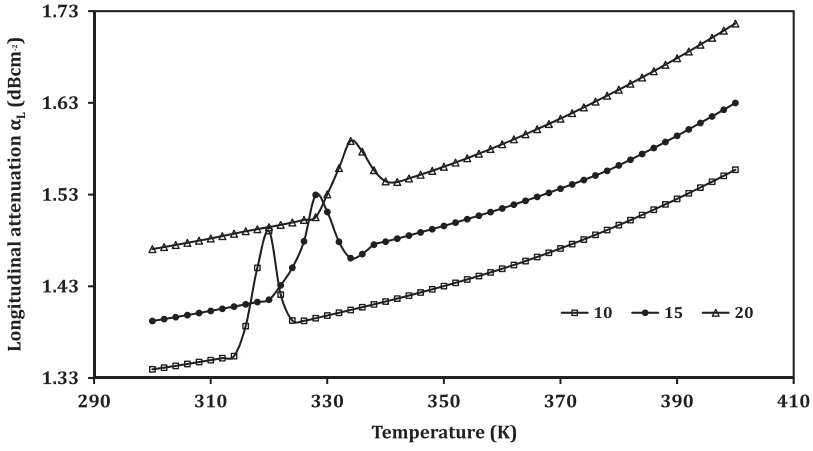

Figure 6. Variation of longitudinal attenuation (α_L) with temperature in the LNMO samples.

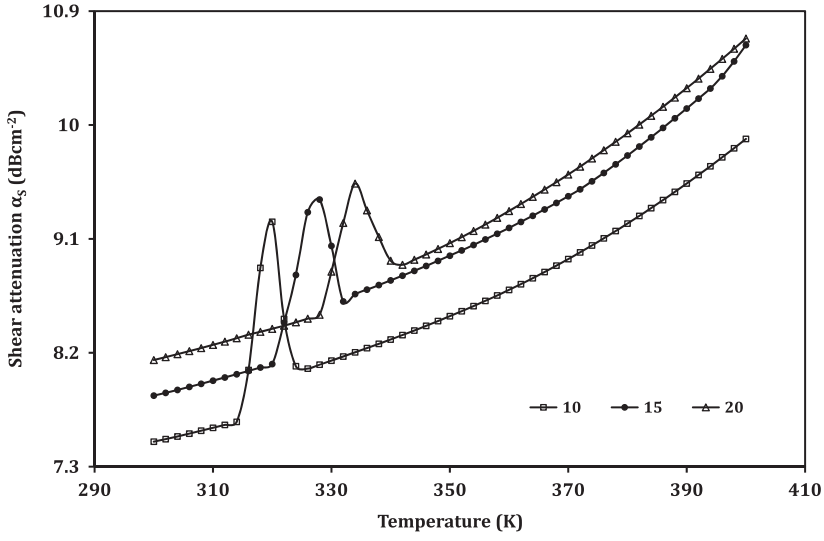

Figure 7. Variation of shear attenuation (α_s) with temperature in the LNMO samples.

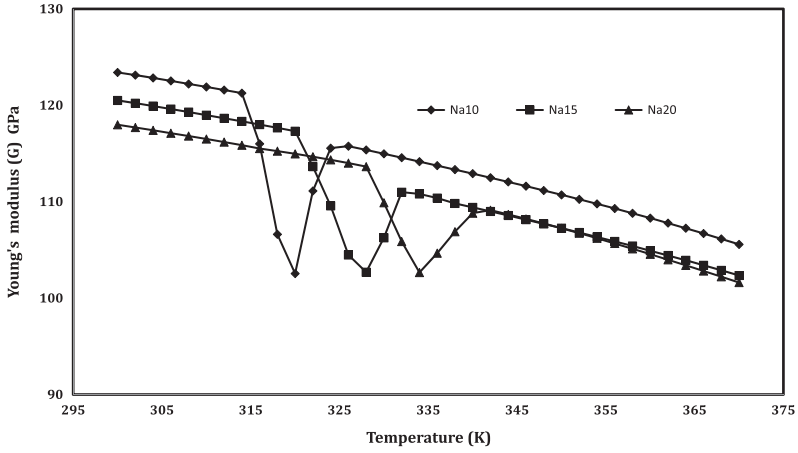

Figure 8. Variation of Young's modulus (*E*) with temperature in the LNMO samples.

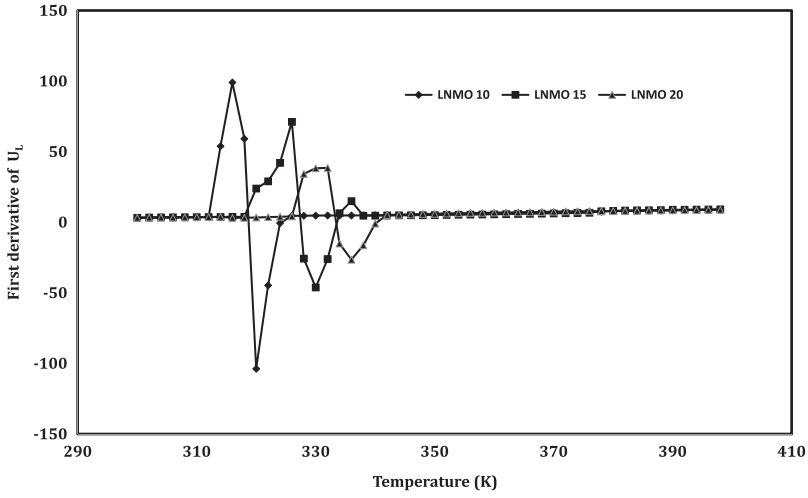

Figure 9. Variation of the first derivative of longitudinal velocity (U_L) with temperature in the LNMO samples.

ultrasonic velocity (U_L) decreases with the increase in temperature monotonically except in a small region. To understand the behaviour of the prepared LNMO perovskite manganite samples, the temperature-dependent curve of U_L is divided into three different regions as shown in Table 2.

In LNMO20 ($La_{0.8}Na_{0.2}MnO_3$) perovskite sample, the region I starts at 300 K and ends at 328 K. The region II lies between 328 and 342 K and the region III occurs between 342 and 400 K. A monotonic decrease in velocity with the increase in temperature is observed in regions I and III. However, the sample shows an anomalous behaviour in region II. At the temperature 328 K, the velocity declines considerably and reaches a minimum at 334 K. Beyond this temperature there is a sharp increase in velocity up to the temperature of 342 K. Once again, in the region III, the velocity shows a monotonic decrease as the temperature increases. The investigation carried out by Zhu et al. (2006) using super conducting quantum interference device (SQUID) magnetometer on $La_{0.8}Na_{0.2}MnO_3$ perovskite manganite sample showed that the FM to PM phase transition takes place at 333 K (i.e. Curie temperature). Correlating the above result with the observations made in the present investigation, it is concluded that the temperatures at which the velocity is minimum (334 K) in the anomalous region are the FM–PM phase transition temperatures (T_c) for the sample LNMO20. Similarly, for samples LNMO10 and LNMO15, the temperatures 320 and 328 K are the FM–PM phase transition temperatures, respectively.

However, the temperature dependence of the attenuation reveals an opposite trend. Instead of a dip followed by a sharp increase in velocity, in the case of attenuation, a peak is observed in the

Table 2. Anomalous region, area of anomalous region, transition width and first derivative of ultrasonic parameters of the LNMO samples

Ultrasonic parameters		LNMO10	LNMO15	LNMO20
Anomalous region	Start *K*	314	320	328
	Anomaly *K*	320	328	334
	End *K*	326	334	342
Area of anomalous region	U_L m/s	2,466.10	2,237.805	1,518.563
	U_S m/s	1,415.28	1,269.819	993.360
	E GPa	114.73	111.866	87.812
Transition width	U_L m s^{-1}	212	166	111
	U_S m s^{-1}	121.5	94.5	72
	α_L dB cm^{-1}	0.0682	0.05715	0.04155
	α_S dB cm^{-1}	0.79055	0.6501	0.5182
	E GPa	15.9603	11.4593	8.7216
First derivative	$\Delta U_L/\Delta T$ m s^{-1} K^{-1}	202.85	117.36	65.0
	$\Delta U_S/\Delta T$ m s^{-1} K^{-1}	117.9476	66.5457	41.1855
	$\Delta\alpha_L/\Delta T$ dBcm^{-1} K^{-1}	0.0664	0.0416	0.02491
	$\Delta\alpha_S/\Delta T$ dBcm^{-1} K^{-1}	0.7876	0.4673	0.2981

anomalous region. A monotonic increase in longitudinal attenuation (α_L) with the increase in temperature is observed in regions I and III. The sample shows an anomalous behaviour in region II. For the LNMO10 sample, at the temperature 314 K, the value of α_L increases steeply and reaches the maximum of 1.4903 dB cm^{-1} at 320 K, then falls sharply up to 326 K. Similarly, the regions obtained for the samples LNMO15 and LNMO20 are listed in Table 2. For samples LNMO15 and LNMO20, the peak values of α_L are obtained at 328 and 334 K, respectively. The peak values of α_L obtained for the perovskite samples LNMO10, LNMO15 and LNMO20 are 1.4903, 1.5297 and 1.5885, respectively, and in the case of α_S, the values are 9.2354, 9.4111 and 9.5369 dB cm^{-1}. This indicates the increase of α_L and α_S with the increase in Na content in the sample. The anomalous peaks in attenuation around T_C indicate the magnetoelastic coupling arising from the spin-phonon coupling in the prepared LNMO perovskite manganite. Further, the coupling is mainly due to linear (single ion) magnetostriction and not volume magnetostriction; the reason is that the peak in attenuation is observed in both longitudinal and shear mode. If it is to be volume magnetostriction, then there should have been no anomaly in the case of shear attenuation (El-Falaky, Gaafar, & El-Aal, 2012; Zhu & Zheng, 1999).

It is seen from the ultrasonic measurements that T_C moves towards a higher value as the composition of Na increases from 10 to 15% and then to 20%. This behaviour is ascribed to the increase in DE interaction caused by the reduction in Mn–O distances. It is due to the increase in average ionic radius of La site produced by the doping of monovalent Na in the perovskite manganite. It is to be noted that ionic radius of La^{3+} is 1.36 Å and that of Na^{1+} is 1.39 Å (Coordination number: 12) (Ye et al., 2001). It is inferred that the distortion of $Mn^{3+}O_6$ octahedral due to JT distortion will come into play. Further, the large difference in valence between La^{3+} and Na^{+} ions in the A site leads to the inhomogeneity in the potential possessed by the e_g electrons as they move through the crystal, leading to some regions with lower potential, in which the e_g electrons can be trapped. Moreover, the substitution of Na^{+} ions for the La^{3+} leads to the formation of the rich Mn^{4+} regions as two Mn^{3+} ions need to be oxidized to Mn^{4+} ions. This favours electronic inhomogeneity and causes phase transition. Hence, the FM–PM transition temperature increases (Roy et al., 2001; Ye et al., 2001) with the doping level of Na content increase.

The temperature dependence of the first derivative of the ultrasonic longitudinal velocity ($\Delta U_L/\Delta T$) is shown in Figure 9. The curves show pronounced peak around the anomalous region. The values

corresponding to the peaks are given in Table 2. One can make use of these values to explore information about the structural and phase transitions that take place in the perovskite materials (Dunaevsky & Deriglazov, 2004). For LNMO10, LNMO15 and LNMO20 perovskite manganite samples, the first derivative of longitudinal velocity ($\Delta U_L/\Delta T$) obtained is 202.85, 117.36 and 65 m s^{-1} K^{-1}, respectively. It indicates that the value of $\Delta U_L/\Delta T$ decreases as the doping level of sodium increases in the LNMO perovskite manganite samples. A similar trend is observed in the case of all the ultrasonic parameters such as shear velocity, longitudinal attenuation and shear attenuation as far as the first derivative is concerned. In the case of longitudinal attenuation, the first derivative values ($\Delta\alpha_L/\Delta T$) are 0.0664, 0.0416 and 0.02491 dB cm^{-1} K^{-1}.

Similar behaviour is exhibited in the case of transition width also. The transition width of the ultrasonic parameters of the prepared LNMO perovskite manganite samples in the anomalous region is given in Table 2. From this table, one can observe that the transition width decreases as the Na content of the samples increases for all the ultrasonic parameters. In the case of shear velocity, the values are 212, 166 and 111 m s^{-1}, respectively, for LNMO10, LNMO15 and LNMO20 perovskite manganite samples. Similarly, the values in shear attenuation are 0.7905, 0.6501 and 0.5182 dB cm^{-1} for LNMO10, LNMO15 and LNMO20 perovskite manganite samples, respectively. Thus, it is clear that as the sodium content of the sample increases, the pronounced peak in the first derivative value as well as the transition width in the temperature dependence of the ultrasonic parameters decreases. The pronounced peak in the value is due to the lattice softening that takes place at the transition temperature. The lattice softening is generally caused by a decrease in velocity and increase in attenuation. So, it is confirmed that in the sample with more doping material, the transition is weakening. The large fluctuations occurring in the lattice volume around the phase transition lead to the anomaly in the ultrasonic parameters shown by the LNMO perovskite samples (Roy et al., 2001).

A strong ingredient of the CMR properties of the perovskites is the local distortion of the $Mn^{3+}O_6$ octahedral that determines the transport properties. The behaviour of the ultrasonic parameters around the anomalous region is caused by the strong coupling between charge, spin, orbital and lattice degrees of freedom and interaction around the transition temperature (Sakthipandi & Rajendran, 2013; Zheng et al., 2002). Hence, it is concluded that these observations offer a solid evidence for coupling and interaction due to the doping of monovalent sodium element in the perovskite manganites.

Moreover, the calculated values of the area of the anomalous regions of the ultrasonic velocities and elastic constants also reveal a similar trend (Table 2). In the case of longitudinal velocity shown in Figure 4, the enclosed area of anomalous region for LNMO10, LNMO15 and LNMO20 perovskite manganite samples is 2,466.10, 2,237.805 and 1,518.503, respectively, and in the case of shear velocity, it is 1,415.28, 1,269.82 and 993.36. The decrease in the area of anomalous region is associated with the enhancing DE interaction between Mn^{3+} and Mn^{4+} ions in the sample. Higher sodium content drives the structure to become more cubic, leading to an increase in one-electron bandwidth. Ultimately, there is greater overlap between O 2p and Mn 3d electrons which causes an increased DE interaction (Roy et al., 2001). Further, the spin-lattice coupling in the magnetic ordering process is the origin of the large change in entropy in the perovskites (Zheng et al., 2002). Hence, one can correlate the change in magnetic entropy to the DE interaction in the rare earth element. The area of the anomalous region is associated with the degree of disorder. Wider area indicates a larger disorder and a narrower area indicates a lesser disorder and lesser change in magnetic entropy (Arunachalam et al., 2015). Thus, the investigation reveals that the magnetic entropy decreases as the doping of sodium content increases in the LNMO samples.

A significant observation revealed in this investigation is the difference in the rate of change in almost all the parameters. In the case of the first derivative of shear velocity ($\Delta U_S/\Delta T$), the difference in value is 51.4019 when the doping level of Na increases from 10 to 15%. But, the difference is much reduced and yields the value 25.3602 only for the same increase in the doping level from 15 to 20%. This behaviour is revealed in almost all the physical and also ultrasonic parameters. It seems that T_C

value will saturate with further increase in the doping level. A possible explanation is the competition between the rhombohedral phase that favours the magnetisation and development of orthorhombic phase that hinders magnetisation. When the doping level of sodium increases, the concentration of Mn^{4+} exceeds to that of Mn^{3+}. This will reduce Mn^{3+}–O–Mn^{4+} pairs in the sample which weaken the DE interaction and favour Mn^{4+}–O–Mn^{4+} super exchange reaction (Roy et al., 2001).

4. Conclusion

In this investigation, perovskite manganite samples LNMO10, LNMO15 and LNMO20 were prepared by the solid-state reaction technique. XRD patterns of the samples confirmed the crystalline nature with a rhombohedral structure. The particle size of the samples was determined from the obtained SEM images. In-situ ultrasonic measurements were carried out on the LNMO samples in the temperature range from 300 to 400 K. Temperature dependence of the ultrasonic parameters was used to find the phase transition temperature in the perovskite samples. The investigation revealed that the FM–PM phase transition temperature (T_c) is 320, 328 and 334 K for LNMO10, LNMO15 and LNMO20 perovskite manganite samples, respectively. The transition temperature T_c increases as the doping concentration of Na increases. Further, in the anomalous region, the transition width and the first derivative of the ultrasonic parameters are found to decrease as the sodium content in the sample increases, indicating the stronger DE interaction, less pronounced lattice softening and decreasing magnetic entropy. As the T_c is around the room temperature, monovalent sodium-doped perovskite manganites may be used for potential applications.

Funding
The authors received no direct funding for this research.

Author details
M. Arunachalam[1]
E-mail: aruntamil1959@gmail.com
P. Thamilmaran[1]
E-mail: thamilmaran62@gmail.com
S. Sankarrajan[2]
E-mail: ssankarrajan@yahoo.co.in
K. Sakthipandi[3]
E-mail: sakthipandi@gmail.com
[1] Department of Physics, Sri S.R.N.M. College, Sattur 626 203, Tamil Nadu, India.
[2] Department of Physics, Unnamalai Institute of Technology, Kovilpatti 628 503, Tamil Nadu, India.
[3] Department of Physics, Sethu Institute of Technology, Kariapatti 626 115, Tamil Nadu, India.

Citation information
Cite this article as: Ultrasonic studies on sodium-doped LaMnO3 perovskite material, M. Arunachalam, P. Thamilmaran, S. Sankarrajan & K. Sakthipandi, *Cogent Physics* (2015), 2: 1067344.

References

Arunachalam, M., Thamilmaran, P., Sankarrajan, S., & Sakthipandi, K. (2015). Study of high temperature metal-insulator phase transition in $La_{1-x}Ca_xMnO_3$ employing *in-situ* ultrasonic studies. *Physica B: Condensed Matter, 456*, 118–124. http://dx.doi.org/10.1016/j.physb.2014.08.033

Chand, U., Kumar, P., & Varma, G. D. (2011). Structural, magnetic and magneto transport properties of $Pr_{1-x}Sr_xMnO_3$ (x = 0.2, 0.3 and 0.05) synthesized by co-precipitation method. *Scholars Research Library Archives of Applied Science Research, 3*, 319–327.

Chen, C. H., & Cheong, S. W. (1996). Commensurate to incommensurate charge ordering and its real-space images in $La_{0.5}$ $Ca_{0.5}$ MnO_3. *Physical Review Letters, 76*, 4042–4045 http://dx.doi.org/10.1103/PhysRevLett.76.4042

Das, S., & Dey, T. K. (2007). Magnetic entropy change in polycrystalline $La_{1-x}K_xMnO_3$ perovskites. *Journal of Alloys and Compounds, 240*, 30–35.

de Gennes, P. G. (1960). Effects of double exchange in magnetic crystals. *Physical Review, 118*, 141–154. http://dx.doi.org/10.1103/PhysRev.118.141

De Teresa, J. M., Blasco, J., Ibarra, M. R., García, J., Marquina, C., Algarabel, P., & del Moral, A. (1995). Giant magnetoresistance in bulk. *Solid State Communications, 96*, 627–630. http://dx.doi.org/10.1016/0038-1098(95)00533-1

Dunaevsky, S. M., Deriglazov, V. V. (2004). Magnetization behavior and metamagnetic transitions in electron-doped manganites induced by a strong magnetic field. *Physics of the Solid State, 46*, 2258–2262. http://dx.doi.org/10.1134/1.1841390

El-Falaky, G. E., Gaafar, M. S., El-Aal, N. S. A. El. (2012). Ultrasonic relaxation in zinc borate glasses. *Current Applied Physics, 12*, 589–596. http://dx.doi.org/10.1016/j.cap.2011.09.009

Jaafar, N. A., & Abd Shukor, R. (2003). Ultrasonic studies on colossal magneto resistive $La_{1-x}Ca_xMnO_3$ (x = 0.25, 0.33 and 0.45). *Physica-B, 334*, 425–431.

Kalyana Lakshmi, Y., Venkataiah, G., Vithal, M., & Venugopal Reddy, P. (2008). Magnetic and electrical behavior of $La_{1-x}A_xMnO_3$ (A=Li, Na, K and Rb) manganites. *Physica B: Condensed Matter, 403*, 3059–3066. http://dx.doi.org/10.1016/j.physb.2008.03.018

Lalitha, G., & Reddy, P. (2009). Elastic behaviour of strontium-doped lanthanum calcium manganites in the vicinity of T_C. *Journal of Physics and Chemistry of Solids, 70*, 960–966. http://dx.doi.org/10.1016/j.jpcs.2009.05.005

Likodimos, V., & Pissas, M. (2005). Magnetic heterogeneity in electron doped La_{1-x} Ca_x MnO_3 manganites studied by means of electron spin resonance. *Journal of Physics: Condensed Matter, 17*, 3903–3914. http://dx.doi.org/10.1088/0953-8984/17/25/017

Millis, A. J. (1995). Double exchange alone does not explain the resistivity of La_{1-x} Sr_x MnO_3. *Physical Review Letters, 74*, 5144–5147. http://dx.doi.org/10.1103/PhysRevLett.74.5144

Park, J. H., Vescovo, E., Kim, H. J., Kwon, C., Ramesh, R., & Venkatesan, T. (1998). Magnetic properties at surface

boundary of a half-metallic ferromagnet $La_{0.7}$ $Sr_{0.3}$ MnO_3. *Physical Review Letters, 81*, 1953–1956. http://dx.doi.org/10.1103/PhysRevLett.81.1953

Paul, L. B., & Paul, M. (2014). The rise of perovskites: The future of low cost solar photo voltaics. *Asia Materials, 6*, 79–83.

Radaelli, P. G., Cox, D. E., Marezio, M., & Cheong, S. W. (1997). Charge, orbital and magnetic ordering in $La_{0.5}Ca_{0.5}MnO_3$. *Physical Review B, 55*, 3015–3023. http://dx.doi.org/10.1103/PhysRevB.55.3015

Roy, S., Guo, Y. Q., Venkatesh, S., & Ali, N. (2001). Interplay of structure and transport properties of sodium-doped lanthanum manganite. *Journal of Physics: Condensed Matter, 13*, 9547–9559.

Sakthipandi, K., & Rajendran, V. (2013). Metal insulator transition of bulk and nanocrystalline $La_{1-x}Ca_xMnO_3$ perovskite manganite materials through *in-situ* ultrasonic measurements. *Materials Characterization, 77*, 70–80. http://dx.doi.org/10.1016/j.matchar.2012.12.013

Taguchi, H. (1998). Electrical properties of functionally graded perovskite type (La, Ca)MnO_3. *Physics Status Solidi A, 170*, 13–117.

Tang, F. L., & Zhang, X. (2006). Jahn–Teller energy dependence of Curie temperature in $La_{1-x}(Ca/Sr)_xMnO_3$. *Journal of Physics Condensed Matter, 18*, 7851–7862. http://dx.doi.org/10.1088/0953-8984/18/34/001

Thamilmaran, P., Arunachalam, M., Sankarrajan, S., & Sakthipandi, K. (2015). On-line ultrasonic characterisation of barium doped lanthanum perovskites. *Physica B: Condensed Matter, 466–467*, 19–25. http://dx.doi.org/10.1016/j.physb.2015.03.017

Tokura, Y. (1997). Metal-insulator phenomena in perovskites of transition metals oxide. *Physica B: Condensed matter, 237–238*, 1–5.

Tovstolytkin, A. I., Pogorily, A. M., & Podyalvski, D. I. (2007). Vacancy-induced enhancement of magnetic interactions in (Ca, Na)-doped lanthanum manganites. *Journal of Applied Physics, 102*, 063902-1–063902-7.

Wang, Z., Xu, Q., Sun, J., Pan, J., & Zhang, H. (2011). Room temperature magnetocaloric effect of La-deficient bulk perovskite manganite $La_{0.7}MnO_3$–δ. *Physica B: Condensed Matter, 406*, 1436–1440. http://dx.doi.org/10.1016/j.physb.2011.01.044

Ye, S. L., Song, W. H., Dai, J. M., Wang, K. Y., Wang, S. G., & Du, J. J. (2001). Large room-temperature magnetoresistance and phase separation in $La_{1-x}Na_xMnO_3$ with 0.1≤x≤0.3. *Journal of Applied Physics, 90*, 2943–2948. http://dx.doi.org/10.1063/1.1396823

Zener, C. (1951). Interaction between the d-shells in the transition metals. II. Ferromagnetic compounds of manganese with perovskite structure. *Physical Review, 82*, 403–405. http://dx.doi.org/10.1103/PhysRev.82.403

Zheng, R. K., Zhu, C. F., Xie, J. Q., Huang, R. X., & Zi, X. G. (2002). Charge transport and ultrasonic properties in $La_{0.57}Ca_{0.43}MnO_3$ perovskite, Matter. *Chemical Physics, 75*, 121–124.

Zhong, W., Chen, W., Ding, W. P., Zhang, N., Hu, A., Du, Y. W., & Yan, Q. J. (1998). Structure, composition and magnetocaloric properties in polycrystalline La A MnO (A = Na, K). *The European Physical Journal B, 3*, 169–174. http://dx.doi.org/10.1007/s100510050298

Zhu, C., & Zheng, R. (1999). Ultrasonic evidence for magnetoelastic coupling in $La_{0.60}Y_{0.07}Ca_{0.33}MnO_3$ perovskites. *Physical Review B, 59*, 11169–11171. http://dx.doi.org/10.1103/PhysRevB.59.11169

Zhu, X., Sun, Y., Dai, J., & Song, W. (2006). Chemical solution deposition and properties of $La_{0.8}Na_{0.1}A_{0.1}MnO_3$ (A = Ca, Na, Sr) films. *Journal of Physics D: Applied Physics, 39*, 2654–2658. http://dx.doi.org/10.1088/0022-3727/39/13/003

***Cogent Physics* (ISSN: 2331-1940) is published by Cogent OA, part of Taylor & Francis Group.**